Open-Cavity Fabry–Perot Interferometer Based on Etched Side-Hole Fiber for Microfluidic Sensing

Shengnan Wu, Guofeng Yan, Bin Zhou, El-Hang Lee, *Fellow, IEEE*, and Sailing He, *Fellow, IEEE*

***Abstract*— An open-cavity fiber-optic Fabry–Perot interferometer (FPI) is designed and demonstrated, with a particular consideration for microfluidic refractive index (RI) sensing. The FPI is composed of an etched side-hole fiber (SHF) sandwiched between two single-mode-fibers. Chemical etching method is used to open up the cavity in the SHF. Experimental results show that an optimal RI sensitivity of more than 1250 nm/RI can be achieved with an open-cavity length of 38 μm for the microfluidic RI range from 1.3400 to 1.3470. In addition, the temperature sensitivity can reach an ultralow level of 1.1 pm/°C. The ease of fabrication, capability for *in situ* measurement, and excellent performance results suggest that the proposed FPI is highly promising as an inline refractometer for temperature-insensitive label-free microfluidic detection and sensing.**

***Index Terms*— Fabry-Perot interferometer, side-hole fiber, microfluidic sensing, temperature cross-sensitivity.**

I. Introduction

DUE to the superior advantages of compact size, high sensitivity and the ability of simultaneous multi-parameter measurement, fiber-optic inline Fabry-Perot interferometers (FPI) have attracted a great deal of attention for physical, chemical and biomedical sensing [1], [2]. In terms of the geometrical aspect, FPIs can be classified either as open-cavity FPIs or as sealed-cavity FPIs. Compared to the open-cavity ones, the sealed-cavity FPIs have been widely developed for different types of applications. In the previous works, a sealed-cavity type FPI with an in line air bubble, attained by fusion technologies, successfully demonstrated the capabilities of high strain sensitivity and very low temperature-cross sensitivity [3], [4]. Similarly, air-sealed FPIs have also been obtained by employing special fibers or tubes such as silica capillaries and photonic crystal fibers [5]–[7]. Solid-cavity fiber FPIs are another kind of sealed-cavity FPIs, which are usually formed by splicing fibers with different material [8]. Some hybrid FP structures were also proposed for simultaneous multi-parameter measurement [9]–[12], [14], [18]. However, sealed-cavity FPIs are not suitable for all kinds of sensing applications, especially in gas/fluidic sensing, due to their limitations of weak light-matter interaction. Viewed from this aspect, open-cavity FPIs have been considered highly promising candidates for Label-free microfluidic sensing applications [13], [14]. Traditionally, micromachining technique has been employed to open up side-holes in fiber by using femtosecond lasers or focused ion beam etching technique [15], [16]. However, the requirements of the high precision machine control and special laser equipment, often result in high cost, limiting the practical applications of the open-cavity FPIs. Recently, a selective etching technique was proposed and demonstrated as an effective, low cost method for production of open-cavity or micro-cell FPI [17]–[20]. The selectivity stems from the different etching rate of different materials. Thus specially doped fibers are always employed, such as P_2O_5 doped fibers [17]–[19], and B-doped polarization-maintaining fibers [20].

In this letter, we propose and experimentally demonstrate an open-cavity fiber-optic Fabry-Perot interferometer which is particularly designed for microfluidic sensing. It is basically composed of an etched SHF sandwiched between two SMFs. Different from the former reports, the selective etching we used here is based on the unique fiber structure. And the smooth surface and the ten-minute etching process endow such FPIs with the advantages of low cost and ease of fabrication. For further microfluidic sensing test, the FPI was integrated with a cross microfluidic slit which was fabricated through photolithography. The refractive index response of the FPI was characterized using sodium hydroxide solution with the RI ranging from 1.3400 to 1.3470. Experimental results show that the FPIs with different open-cavity lengths display similar linear RI responses with different RI sensitivities. Due to the strong light-matter interaction, the optimal RI sensitivity of more than 1251 nm/RI can be achieved with an open-cavity length of 38 μm, which is about 8 times larger than the reported value of the etched panda fiber based fiber interferometer [20]. The temperature response was also

Manuscript received April 7, 2015; revised May 26, 2015; accepted June 6, 2015. Date of publication June 15, 2015; date of current version July 29, 2015. This work was supported in part by the National High Technology Research and Development Program of China under Grant 2012AA012201, in part by the Program of Zhejiang Leading Team of Science and Technology Innovation under Grant 2010R50007, in part by the 111 Project, and in part by the National Natural Science Foundation of China under Grant 91233208.

S. Wu, G. Yan, and E.-H. Lee are with the State Key Laboratory of Modern Optical Instrumentation, Centre for Optical and Electromagnetic Research, Department of Optical Engineering, Zhejiang University, Hangzhou 310058, China (e-mail: wushengnan@zju.edu.cn; yanguofeng@zju.edu.cn; ehlee12@zju.edu.cn).

B. Zhou is with the South China Academy of Advanced Optoelectronics, South China Normal University, Guangzhou 510631, China (e-mail: zhoubin_mail@163.com).

S. He is with the State Key Laboratory of Modern Optical Instrumentation, Centre for Optical and Electromagnetic Research, Department of Optical Engineering, Zhejiang University, Hangzhou 310058, China, and also with the Department of Electromagnetic Engineering, School of Electrical Engineering, Royal Institute of Technology, Stockholm 10044, Sweden (e-mail: sailing@zju.edu.cn).

Color versions of one or more of the figures in this letter are available online at http://ieeexplore.ieee.org.

Digital Object Identifier 10.1109/LPT.2015.2443375

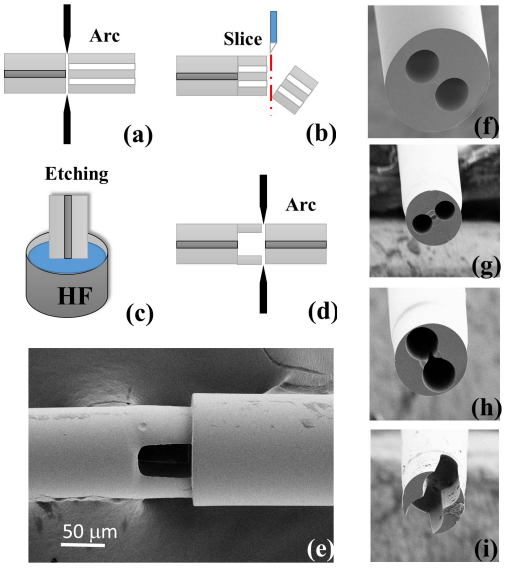

Fig. 1. (a), (b), (c) and (d) Schematic diagram of the fabrication process of this FPI. (f) Scanning electron microscope (SEM) image of the SHF we used, (g), (h) and (i) SEM images of the SHF end with etching time of 5 min, 8 min and 15 min, respectively. (e) SEM image of the final FPI structure.

investigated and it shows that the FPIs exhibit an ultra-low temperature cross-sensitivity of 1.1 pm/°C for a cavity length of 38 μm. The results show that the proposed FPI is an outstanding candidate for Label-free and temperature-insensitive biochemical microfluidic sensing applications.

II. Fabrication and Operating Principles

A. Fabrication

The SHF used in our study is a kind of microstructured fiber manufactured by the Yangtze Optical Electronics Co., Ltd, China, and its cross section is shown in Fig. 1(f). It contains two air holes with diameters of 43 μm, symmetrically located on both sides of the germanium doped fiber core having a diameter of 9 μm. This unique geometry provides us with an easy way to open up a cavity in the SHF, simply by employing time-controlled chemical etch method. The schematic diagram of the FPI fabrication process is shown in Fig. 1(a)∼(d). First, a piece of SHF was spliced to a standard SMF (SMF-28) by using a commercial fusion splicer (FIFEL S177) under the 'Manual' operation mode. In order to avoid the collapse of the holes in the SHF, a low power and a short duration of the arc discharge were optimally selected and applied (see Fig. 1(a)). Second, as shown in Fig. 1(b), the SHF tail was sliced to the sizes of tens of microns with the help of a microscope. The resultant SMF-SHF structure was then immersed into 40% hydrofluoric (HF) acid solution for chemical etching. Due to the capillary effect, the HF acid filled the air holes automatically. As a result, the etching process took place both on the inside surface and the outside surface of the SHF. This step is the key part of the whole fabrication process and the microscopy was used to monitor the etching process *in situ*. Since the thickness of the cross section differs at different location, after a certain etching time, the thinner wall disappeared first while the thicker wall remained. Thus, by precisely controlling the etching time, a side-open cavity can be finally formed. The scanning electron microscope (SEM) was used to characterize the etched SHF ends for different etching time of 5 min, 8 min and 15 min, respectively. The SEM images shows the three discrete formations of the air-hole cavity (see Fig. 1(g) to (i)) which started from the inner fiber core to the fiber cladding due to the lower binding energy compared to the silica cladding walls. A smooth surface and well-formed cavity were also confirmed. Finally, as shown in Fig. 1(d), the side-open SHF was spliced to a standard SMF again by using the same fusion parameters as used in step 1. The SEM image of the fabricated FPI sample is shown in Fig. 1(e). We can clearly see the FPI maintaining an open channel between two SMFs and the diameter mismatch between the two SMFs caused by the chemical etching process.

B. Operating Principle

The air cavity existing between the SMFs has two splicing interfaces which also function as two mirrors. The two beams reflected by each mirror will interfere when they are coupled into the leading SMF. Thus the reflection intensity I of the interference fringes can be expressed as:

$$I = I_1 + I_2 + 2\sqrt{I_1 I_2}\cos\left(\frac{4\pi n_m L}{\lambda_D} + \phi_0\right) \tag{1}$$

where I_1 and I_2 are the intensities of the light reflected by the two mirrors; n_m is the refractive index of the medium in the cavity; L is the cavity length and ϕ_0 is the initial phase difference between the two reflected light beam. The destructive interference dip occurs, when the phase condition satisfies that:

$$\frac{4\pi n_m L}{\lambda_D} + \phi_0 = (2k+1)\pi \tag{2}$$

where λ_D is the dip wavelength of the interference fringes and k is an integer. Hence, we can see that the dip wavelength is a function of n_m. The free spectral range (FSR) of the spectrum can be calculated as:

$$FSR \approx \frac{\lambda_1 \lambda_2}{2 n_m L} \tag{3}$$

where λ_1 and λ_2 are the wavelengths at the two adjacent dips of the interference fringes.

Differentiating Eq. (2) with respect to n_m, we can get

$$\frac{d\lambda_D(n_m)}{dn_m} = \frac{\lambda_D(n_m)}{n_m} = \frac{4\pi L}{(2k+1)\pi - \phi_0} \tag{4}$$

here k is a constant for a certain order interference dip. Thus the dip wavelength shift is proportional to the variation of n_m. The linear RI response greatly improves the measurement accuracy and makes the measurement more easily.

III. Experimental Results and Discussion

A. Different Cavity Length

In the experiment, we fabricated three FPI samples with different cavity lengths of 38 μm, 56 μm and 123 μm, respectively. The robustness of the fabricated FPI was characterized by strain response test and the insertion loss in air at wavelength of 1550 nm was also measured. The

TABLE I
CHARACTERISTICS OF STRAIN AND INSERTION LOSS

Length (μm)	Strain sensitivity (pm/με)	Limit stain (με)	Insertion loss (dB)
38	7.57	7500	5.46
56	4.73	7000	9.07
123	1.31	7100	20.13

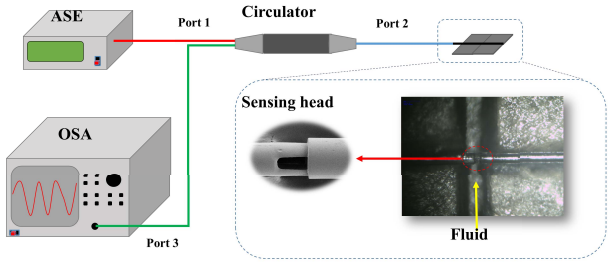

Fig. 2. Schematic diagram of the experimental set up for characterization of the microfluidic refractive index response.

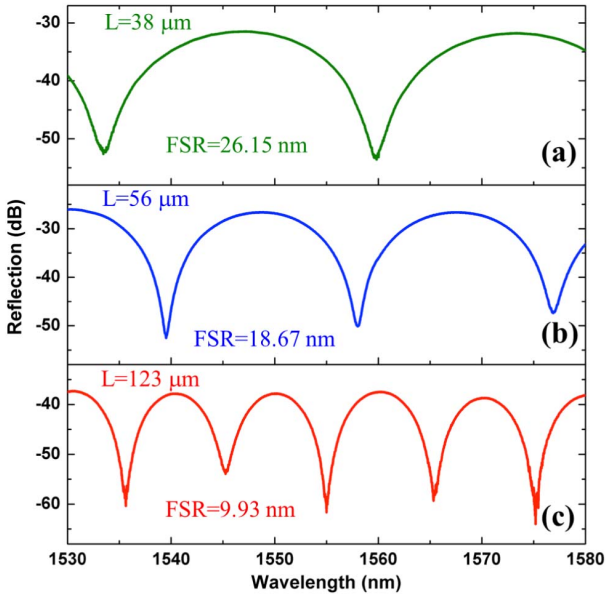

Fig. 3. Reflection spectra of FPI samples measured in air for different cavity lengths of (a) 38 μm, (b) 56 μm and (c) 123 μm.

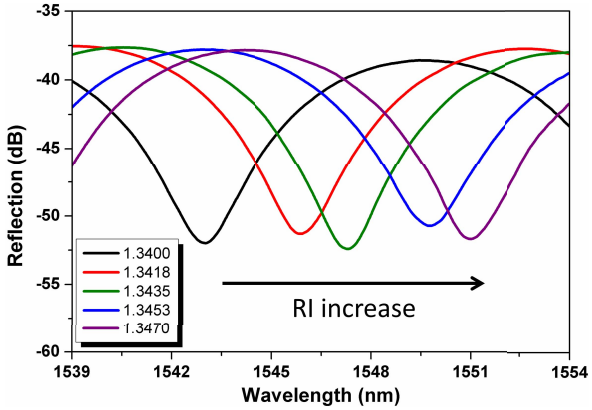

Fig. 4. Experimental results of microfluidic spectral response of FPI with cavity length of 56 μm.

results are given in Table. 1. Naturely, the longer cavity length consists longer thin wall section, which leads to lower strain sensitivity and limit strain. To enhance the mechanical strength, in the following test, the FPI was integrated into a microfluidic chip. Insertion loss was mainly caused by the reflection and scattering at the air-silica interfaces, and the recoupling efficient of the downstream SMF. The Longer cavity length will significantly decrease the recoupling efficient due to the light beam expansion, leading to larger insertion loss.

Figure 3 shows the reflection spectra of these samples in air. The spectrum was measured by using a broadband light source with an output wavelength range from 1200 nm to 1650 nm, a circulator and an optical spectrum analyzer (ANDO, AQ6317) with resolution of 0.01 nm (see Fig. 2). The results show that, when the cavity length increases from 38 μm to 123 μm, the FSR decreases from 26.15 nm to 9.93 nm and the bandwidth of the resonance dip decreases from 1.24 nm to 0.2 nm. Since a larger FSR provides a wider measurement range and a smaller bandwidth offers a higher measurement accuracy, there lies a tradeoff in selecting the open-cavity length. What's more, the extinction ratios of all the spectra are more than 20 dB, surpassing most of the existing open cavity FPIs [13], [14].

B. Microfluidic RI Response

The main advantage of the open cavity FPI is the ability for microfluidic *in situ* measurement. A microfluidic chip was fabricated by embedding the FPI into a slit with a microfluidic channel just crossing the open cavity (see Fig. 2). The sodium hydroxide solution with RI in the range of 1.3400 to 1.3470 was prepared in advance and was injected in steps into the micro-channel as microfluidic samples to characterize the refractive index response of the FPIs. Here, the refractive indexes corresponding to the employed solutions all refer to their values at the wavelength of 589.3 nm.

The spectral response of the FPI sample with a cavity length of 56 μm is presented in Fig. 4. Consistent with the analytical result from Eq. 5, the dip of the spectrum red-shifts linearly with respect to the increase of the liquid's RI. For comparison, the wavelength shifts of the dips around 1550 nm are plotted in Fig. 5 as a function of RI changes for cavity lengths of 38 μm, 56 μm, and 123 μm, respectively. The linear fit process was conducted to estimate the RI sensitivities and one can clearly obtain the sensitivities of 1059 nm/RI, 1138 nm/RI and 1251 nm/RI for FPIs with cavity length of 123 μm, 56 μm and 38 μm, respectively. This result clearly suggests that a higher RI sensitivity can be achieved by simply employing a short FPI cavity length for an operation wavelength around 1550 nm.

C. Temperature Response

The intrinsic temperature response of the fabricated samples was measured by using a tunable oven. Each setting temperature is kept at least 5 min to eliminate the influence of the temperature fluctuation. The reflection spectra were recorded at a temperature interval of 20 °C. The measurement results are shown in Fig. 6. The fabricated FPI samples show

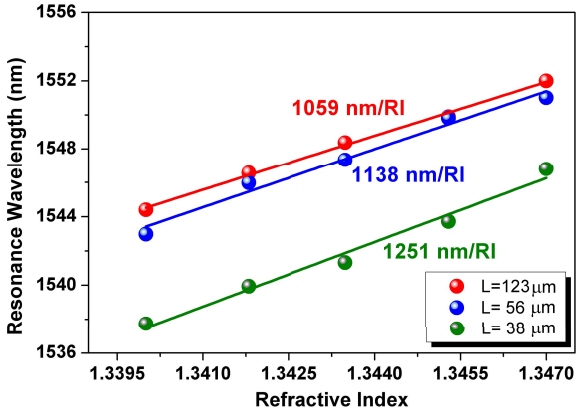

Fig. 5. Wavelength shift of the dip as a function of RI for different cavity length of 38 μm, 56 μm and 123 μm, respectively.

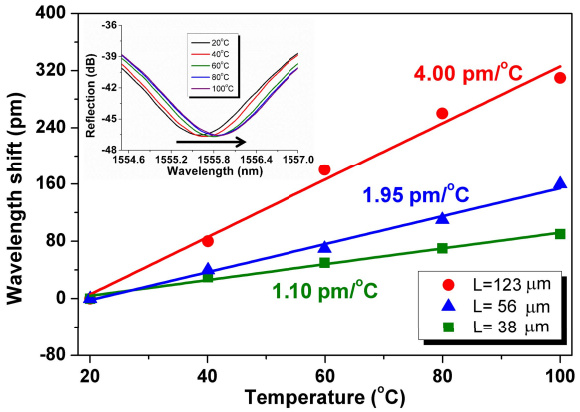

Fig. 6. Temperature response of the dip wavelength for different cavity lengths of 38 μm, 56 μm and 123 μm respectively. Inset: Spectral evolution of the FPI with cavity length of 56 μm.

linear responses with the changes of ambient temperature. Such variation is due to the temperature induced RI changes and thermo-expansion of the fiber. The intrinsic temperature sensitivities calculated by the linear fit show 4.00 pm/°C, 1.95 pm/°C, and 1.10 pm/°C, corresponding to the FPIs with cavity lengths of 123 μm, 56 μm and 38 μm, respectively. Then the temperature induced RI measurement error is found to be at an ultra-low level of $8.8\times10^{-7}RIU$, comparable with those of other high performance FPIs [13], [21]. It is strongly suggesting that such FPI sensors also have great potential in characterizing the thermo-optic coefficient of fluids.

IV. Conclusion

A novel open-cavity all-fiber FPI has been designed, fabricated and demonstrated. This structure can be readily obtained by simply etching the SHF and sandwiching it between two SMFs. The microfluidic RI measurement and temperature response were carried out and a high RI sensitivity of 1250 nm/RI and low intrinsic temperature sensitivity of 1.10 pm/°C were experimentally obtained. The ease of fabrication, high linear RI sensitivity and negligible temperature cross-sensitivity suggest that such an open-cavity FPI integrated with a microfluidic chip will be a highly promising platform for a variety of bio-chemical *in situ* sensing applications.

Acknowledgment

Many thanks for the help of Zhenggang Lian, Hongbo Wei and Xiang Chen from the Yangtze Optical Electronics Co., Ltd., China, to supply us sidehole fibers. Also thanks to Prof. Youngjoo Chung's group to send us some homemade sidehole fibers.

References

[1] Y.-J. Rao, "Recent progress in fiber-optic extrinsic Fabry–Pérot interferometric sensors," *Opt. Fiber Technol.*, vol. 12, no. 3, pp. 227–237, Jul. 2006.
[2] B. H. Lee *et al.*, "Interferometric fiber optic sensors," *Sensors*, vol. 12, no. 3, pp. 2467–2486, Mar. 2012.
[3] S. Liu *et al.*, "High-sensitivity strain sensor based on in-fiber improved Fabry–Pérot interferometer," *Opt. Lett.*, vol. 39, no. 7, pp. 2121–2124, Apr. 2014.
[4] C. Yin *et al.*, "Temperature-independent ultrasensitive Fabry–Pérot all-fiber strain sensor based on a bubble-expanded microcavity," *IEEE Photon. J.*, vol. 6, no. 4, Aug. 2014, Art. ID 6802009.
[5] Y. Du *et al.*, "A miniature Fabry–Pérot interferometer for high temperature measurement using a double-core photonic crystal fiber," *IEEE Sensors J.*, vol. 14, no. 4, pp. 1069–1073, Apr. 2014.
[6] D. Lee, M. Yang, C. Huang, and J. Dai, "Optical fiber high-temperature sensor based on dielectric films extrinsic Fabry–Pérot Cavity," *IEEE Photon. Technol. Lett.*, vol. 26, no. 21, pp. 2107–2110, Nov. 1, 2014.
[7] M. Deng, C.-P. Tang, T. Zhu, and Y.-J. Rao, "PCF-based Fabry–Pérot interferometric sensor for strain measurement at high temperatures," *IEEE Photon. Technol. Lett.*, vol. 23, no. 11, pp. 700–702, Jun. 1, 2011.
[8] L. Li *et al.*, "Ultrahigh sensitive temperature sensor based on Fabry–Pérot interference assisted by a graphene diaphragm," *IEEE Sensors J.*, vol. 15, no. 1, pp. 505–509, Jan. 2015.
[9] S. Pevec and D. Donlagic, "Miniature fiber-optic sensor for simultaneous measurement of pressure and refractive index," *Opt. Lett.*, vol. 39, no. 21, pp. 6221–6224, Nov. 2014.
[10] A. Zhou *et al.*, "Hybrid structured fiber-optic Fabry–Pérot interferometer for simultaneous measurement of strain and temperature," *Opt. Lett.*, vol. 39, no. 18, pp. 5267–5270, Sep. 2014.
[11] H. Bae, D. Yun, H. Liu, D. A. Olson, and M. Yu, "Hybrid miniature Fabry–Pérot sensor with dual optical cavities for simultaneous pressure and temperature measurements," *J. Lightw. Technol.*, vol. 32, no. 8, pp. 1585–1593, Apr. 15, 2014.
[12] J. Yin *et al.*, "Batch-producible fiber-optic Fabry–Pérot sensor for simultaneous pressure and temperature sensing," *IEEE Photon. Technol. Lett.*, vol. 26, no. 20, pp. 2070–2073, Oct. 15, 2014.
[13] C. Wu, Z. Liu, A. P. Zhang, B. O. Guan, and H. Y. Tam, "In-line open-cavity Fabry–Pérot interferometer formed by C-shaped fiber fortemperature-insensitive refractive index sensing," *Opt. Exp.*, vol. 22, no. 18, pp. 21757–21766, Sep. 2014.
[14] S. Gao *et al.*, "Microfiber-enabled in-line Fabry–Pérot interferometer for high-sensitive force and refractive index sensing," *J. Lightw. Technol.*, vol. 32, no. 9, pp. 1682–1688, May 1, 2014.
[15] T. Wei, Y. Han, Y. Li, H.-L. Tsai, and H. Xiao, "Temperature-insensitive miniaturized fiber inline Fabry–Pérot interferometer for highly sensitive refractive index measurement," *Opt. Exp.*, vol. 16, no. 8, pp. 5764–5769, Apr. 2008.
[16] T. Ming, P. Lu, L. Chen, D. Liu, and M. Yang, "Micro multicavity Fabry–Pérot interferometers sensor in SMFs machined by femtosecond laser," *IEEE Photon. Technol. Lett.*, vol. 25, no. 16, pp. 1609–1612, Aug. 15, 2013.
[17] D. Donlagic, "All-fiber micromachined microcell," *Opt. Lett.*, vol. 36, no. 16, pp. 3148–3150, Aug. 2011.
[18] S. Pevec and D. Donlagic, "High resolution, all-fiber, micro-machined sensor for simultaneous measurement of refractive index and temperature," *Opt. Exp.*, vol. 22, no. 13, pp. 16241–16253, Jun. 2014.
[19] E. Preter, B. Preloznik, V. Artel, C. N. Sukenik, D. Donlagic, and A. Zadok, "Monitoring the evaporation of fluids from fiber-optic micro-cell cavities," *Sensors*, vol. 13, no. 11, pp. 15261–15273, Nov. 2013.
[20] H. Tang, J. Zhu, H. Yin, R. Wang, H. Wang, and B. Yu, "Optical fiber refractometer based on etched-stress applying parts PANDA fiber," *IEEE Photon. Technol. Lett.*, vol. 26, no. 13, pp. 1356–1359, Jul. 1, 2014.
[21] C. Wu, M.-L. V. Tse, Z. Liu, B.-O. Guan, C. Lu, and H.-Y. Tam, "In-line microfluidic refractometer based on C-shaped fiber assisted photonic crystal fiber Sagnac interferometer," *Opt. Lett.*, vol. 38, no. 17, pp. 3283–3286, Sep. 2013.